NANO LETTERS

Letter

pubs.acs.org/NanoLett

Programmable Redox State of the Nickel Ion Chain in DNA

Hsueh-Liang Chu,[†] Shao-Chien Chiu,[‡] Ching-Feng Sung,[‡] Wellen Tseng,[†] Yu-Chuan Chang,[†] Wen-Bin Jian,[*,‡] Yu-Chang Chen,[*,‡,§] Chiun-Jye Yuan,[†] Hsing-Yuan Li,[†] Frank X. Gu,[∥] Massimiliano Di Ventra,[⊥] and Chia-Ching Chang[*,†,#]

[†]Department of Biological Science and Technology, National Chiao Tung University, 75 Bo Ai Street, Hsinchu, Taiwan, 30068

[‡]Department of Electrophysics, National Chiao Tung University, 1001 Ta Hsueh Road, Hsinchu, Taiwan, 30050

[§]National Center of Theoretical Physics, National Chiao Tung University, 1001 Ta Hsueh Road, Hsinchu, Taiwan, 30050

[∥]Department of Chemical Engineering, Waterloo Institute for Nanotechnology, University of Waterloo, 200 University Ave West, Waterloo, Ontario, Canada N2L3G1

[⊥]Department of Physics, University of California, San Diego, United States

[#]Institute of Physics, Academia Sinica, 128 Academia Road, Section 2, Nankang, Taipei, Taiwan, 11529

Supporting Information

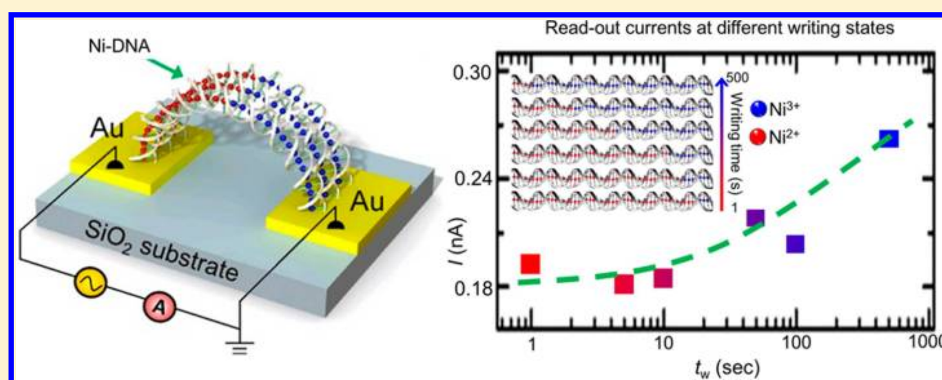

ABSTRACT: DNA is a nanowire in nature which chelates Ni ions and forms a conducting chain in its base-pairs (Ni-DNA). Each Ni ion in Ni-DNA exhibits low (Ni^{2+}) or high (Ni^{3+}) oxidation state and can be switched sequentially by applying bias voltage with different polarities and writing times. The ratio of low and high oxidation states of Ni ions in Ni-DNA represents a programmable multistate memory system with an added capacitive component, in which multistate information can be written, read, and erased. This study also indicates that the biomolecule-based self-organized nanostructure can be used as a template for nanodevice fabrication.

KEYWORDS: *DNA, Ni-DNA, nanowire system, multistate memory effect, memory resistance systems, nanotemplate*

DNA is a quasi-one-dimensional nanomaterial with properties of self-assembly and length controllable by biosynthesis.[1−5] Although the electron transfer properties of DNA have been studied intensely, the conclusions on DNA conductance have remained controversial. Conducting,[2] semiconducting,[6] and insulating[7] properties of DNA have all been proposed. Although previous studies cannot provide a convincing mechanism for the intrinsic conductance of DNA, it is well-known that DNA conductance/redox functions increases dramatically upon doping with Ni ions.[3,4,8,9] The electrical property of Ni-DNA has been characterized via atomic force microscopy (AFM), demonstrating that Ni-DNA acts as a conducting nanowire.[4,10] The incorporation of Ni ions may result in a reduction of the original DNA band gap, evidenced by a redshift of the UV absorption spectra.[11,12] Thus, the incorporation of Ni ions converts native DNA into a conducting wire and allows charge transport via the $\pi-\pi$ stacking corridor.[9] It has also been demonstrated that Ni-DNA acts like a conducting wire with an insulated shell to prevent intermolecular electron leakage.[9] Furthermore, the device with the Ni^{2+}-chelated DNA (Ni-DNA) connecting two gold electrodes exhibited a negative differential resistance (NDR) behavior, when the measurement of current response in a cyclic-voltage scan ($I-V$) was performed under an ambient and water-free condition.[3] This cyclic $I-V$ switching is one of the key mechanisms for memory devices.[13]

A memristive system is the resistance of the system which varies according to the "history" of applied voltage or currents.[14] The expression of memristive effects by the material can be determined in part by the presence of hysteresis such as

Received: December 12, 2013
Revised: January 9, 2014
Published: January 21, 2014

 © 2014 American Chemical Society

that induced by NDR.[15] In a previous study on memristive system, characteristics of the memory resistor were achieved on a solid-state device based on the variation of the boundary between the high and low-resistance layers of titanium dioxide (TiO_2) and TiO_{2-x}.[15] This system could store at least twice as much data in the same area.[15] Additionally, memristive systems can be used in digital logic as programmable switches in switching blocks.[16,17] Herein, we demonstrate that the resistance of Ni-DNA depends on the "history" of applied voltage or currents; that is, Ni-DNA behaves as a memristive system.

To fabricate the Ni-DNA memristor device, linear DNA strands (2189 bp) were obtained from Rop-tat plasmid[18] by BamHI and EcoRI digestion, and the DNA strands were chelated with Ni ions using our previously established approaches.[4,9] The Ni-DNA molecules were linked on two gold electrodes through the Ni ions chelated BamHI and EcoRI linkers; those were self-assembled on the gold electrodes. The residue water on the Ni-DNA device was removed by baking at 80 °C for 15 min (see the Experimental Section and Supporting Information, SI). The nanogold electrodes were fabricated using a standard procedure described in the Experimental Section and SI (Figure S1). The electrical properties of the electrodes were measured via a high-impedance electrometer (Keithley 6517b, Kiethley, USA). Two probes were utilized to acquire data for the current−voltage ($I-V$) curves and to monitor the device performance of the Ni-DNA memristor. The current flowing through the Ni-DNA could be measured when bias voltage was supplied.

Previous studies have shown that divalent metal ions can bind to double helix DNA at high pH by replacing the imide protons of the guanosine and thymidine units (Figure S2a). The formation of Ni-DNA inhibited the fluorescent DNA dye SYBR green from intercalating into stacking spaces between DNA base pairs.[4] However, the Ni ions can be removed by ethylenediaminetetraacetic acid (EDTA; Figure S2b). These results indicate that the Ni ion was coordinated to the DNA at pH 9 and that the Ni ion chelating process is reversible. To use Ni-DNA as a conductor, the self-assembled monolayers (SAMs) of Ni-DNA linkers and Ni-DNA bridges were formed as described in the Experimental Section and SI, and the structure of the device was validated by AFM analysis (Figure 1).

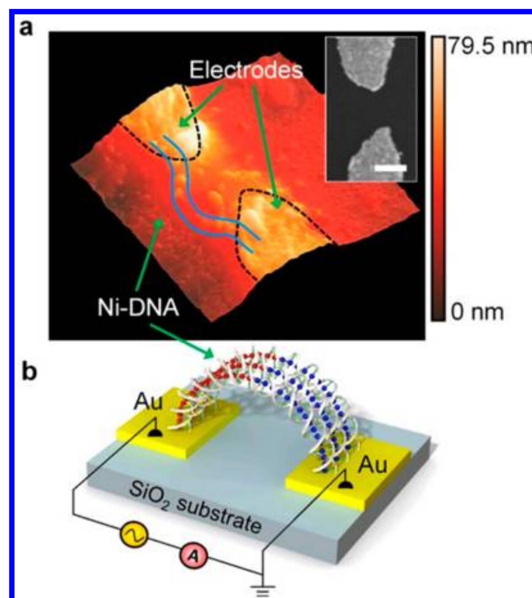

Figure 1. (a) AFM image of the Ni-DNA device. The inset shows the electrodes before DNA deposition. (b) The schematic shows the Ni-DNA device system. Red spheres denoted Ni^{2+} ions, and blue spheres denoted the Ni^{3+} ions.

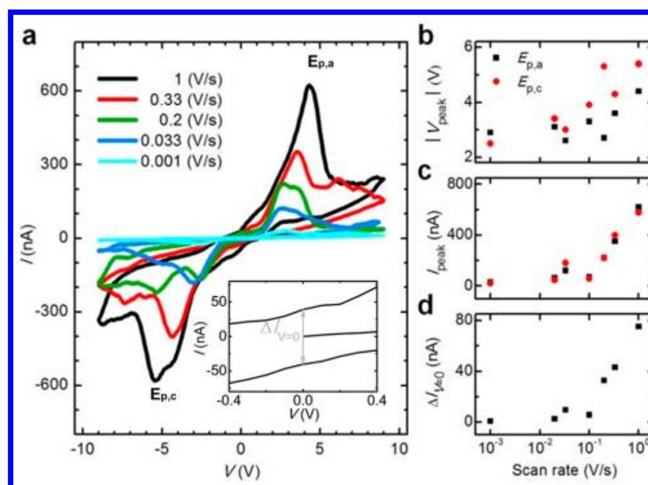

Figure 2. (a) Cyclic sweeping of $I-V$ characteristics of the Ni-DNA memory device in the voltage range from −9 to +9 V at various scanning rates. The inset highlights the current difference at zero voltage ($\Delta I_{V=0}$), where the starting line of $I-V$ sweeping at zero current is presented for comparison. Scan rate dependences of the oxidation ($E_{p,a}$) and reduction ($E_{p,c}$) voltages (b), the peak current, I_{peak}, in positive and negative sweepings (c), and the zero voltage current, $\Delta I_{V=0}$ (d), are extracted from data in part a.

Figure 2a shows the scan rate dependence of the $I-V$ loops of the Ni-DNA device. The $I-V$ curves show an obvious NDR effect with a hysteresis loop that indicates the appearance of a memristive system.[14] In our previous study, we verified that the NDR effect is attributed to the redox reaction between Ni^{2+} and Ni^{3+} within the DNA base pairs.[3] By sweeping the voltage from 0 to +9 V at a speed of 1 V/s (see Figure 2a), the current increased and reached a maximum at a voltage ($E_{p,a}$) of approximately 4.4 V, which is indicative of the oxidation of the Ni ion (from Ni^{2+} to Ni^{3+}). The current decreased at higher voltages and was further reduced when the voltage was swept from +9 V back to 0 V. A nonzero current was observed when the voltage was swept back to zero, which is different from the initial condition of zero current at zero voltage (see inset of Figure 2a). This hysteresis current arises from the capacitance of Ni-DNA, which will be discussed later. A further sweep from 0 V to −9 V produced another current peak ($E_{p,c}$) at a voltage of approximately −5.6 V that represented the reduction of Ni^{3+} back to Ni^{2+}. Notably, the cyclic redox reactions shown in Figure 2a has never been observed in native DNA devices (see SI, Figure S3). This phenomenon is consistent with our previous report.[3] Figure 2a also shows the scan rate dependence of the $I-V$ loops. The magnitude of the peak current, $E_{p,a}$ or $E_{p,c}$, also increased with a faster sweeping speed. The dependence of the oxidation/reduction voltage, peak current, and nonzero current at zero voltage on the scan rate are summarized in Figure 2b−d. All three figures show monotonic increment behavior with an increase of the scanning speed. This scan rate dependence is probably attributed to the variation of the redox rate with Ni ions.

As noted above, the resistance of Ni-DNA device system varies with the history of applied voltage or current. To explain

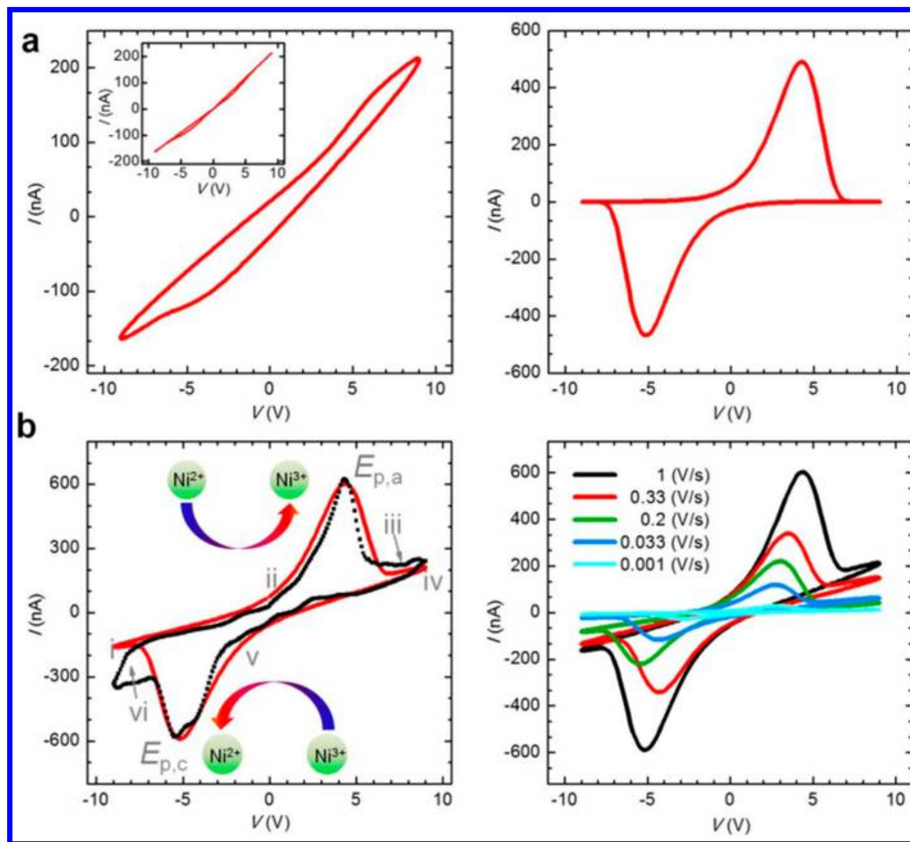

Figure 3. (a) Simulated cyclic $I-V$ characteristics due to I_{drift} (left panel) and $\tilde{I}$ (right panel). The parameters chosen for this simulation are: $E_{ox} = E_{red} = 3.5$ eV, $k_{ox}^0 = 0.018\ s^{-1}$, $k_{red}^0 = 0.00013\ s^{-1}$, $C_{2+} = 448$ nF, $C_{3+} = 717$ nF, $\phi = 0.025\pi$ rad, $f = 5.3 \times 10^6$, $\beta = 1/2$, and $\alpha \approx k_B/27$, where $k_B = 8.6 \times 10^{-5}$ eV/K is the Boltzmann constant. The inset of the left panel shows the cyclic $I-V$ characteristics due to I_{drift} with the phase angle $\phi = 0$. (b) Comparison of simulated (red line) cyclic $I-V$ characteristics with the experimental data (black line) at scan rate of 1 V/s and $T = 300$ K (left panel) and simulated cyclic $I-V$ characteristics of the Ni-DNA memory device in the voltage range of −9 to +9 V at various scanning rates (right panel).

the resistive memory effect, we propose a capacitive memristor model to illustrate the $I-V$ characteristics of the Ni-DNA device system. Memristive systems can be defined in terms of the following equations:[14]

$$V = R(w, i)i \tag{1}$$

and

$$\frac{dw}{dt} = f(w, i) \tag{2}$$

where w is a set of state variables, and R and f are explicit functions of time.

The current through the Ni-DNA device triggers redox reactions of nickel ions embedded in the DNA:

$$Ni^{2+} \underset{\text{reduction}}{\overset{\text{oxidation}}{\longleftrightarrow}} Ni^{3+} + e^- \tag{3}$$

The oxidation−reduction processes change the number of high (Ni^{3+}) or low (Ni^{2+}) oxidative Ni ions in Ni-DNA due to the alternating current flowing between the left and the right electrodes. The emission and absorption of electrons caused by the oxidation−reduction processes initiate charge accumulation in the Ni-DNA region, forming a source of capacitance. We model the Ni-DNA system depicted in Figure 1b as a resistor−capacitor network, as shown in Figure S4. In the absence of capacitors, the total resistance of the Ni-DNA device is proportional to the number of Ni^{2+} and Ni^{3+} ions, similar to the case of the TiO_{2-x} memristive system proposed by the HP Laboratory.[15]

Compared with a current of the order of mA in the TiO_{2-x} memristive system, the Ni-DNA device has a large resistance with a current at the order of nA, the consequence of which is non-negligible components of the current caused by the charge accumulation. The charge accumulation introduces a capacitive impedance and also a phase in the current with respective to the voltage. Under these circumstances, a nonvanishing current is observed at zero bias in the hysteresis $I-V$ curve. A drift-diffusive model for the resistor−capacitor network is proposed to explain the unsual noncrossing current−voltage hysteresis loop in the Ni-DNA system. The current comprises a combination of the drift current $I_{drift}(t)$ and diffusive current $\tilde{I}(t)$,

$$I(t) = I_{drift}(t) + \tilde{I}(t) \tag{4}$$

For details, please see the SI.

The drift current $I_{drift}(t)$ is driven by the external voltage, $V(t) = V_0 \sin(\omega t)$, due to the impedance of the resistor−capacitor network,

$$I_{drift}(t) = \frac{v(t + \phi)}{z(t)} \tag{5}$$

where ϕ is the phase angle due to the charge accumulation. $Z(t)$ is the impedance of the resistor−capacitor network shown in Figure S4,

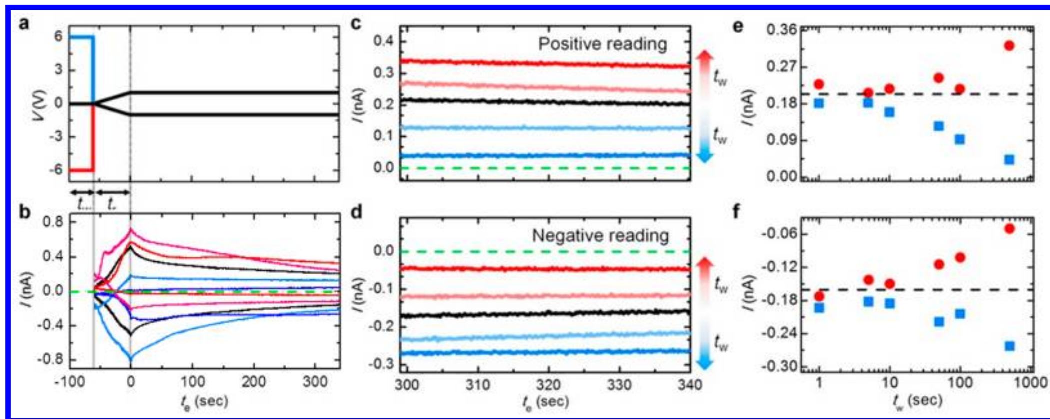

Figure 4. (a) t_w and t_r indicate the writing and ramp-up time. The black line in the t_w indicates nonbias application. The reading voltage was set at +1 V (−1 V). The blue and red lines mark positive and negative bias writings, respectively. (b) The read-out current as a function of the elapsed time, t_e. The upper (lower) black line presents the reference current of the positive (negative) reading for Ni-DNA device. The curves in dark red, light red, black, light blue, and dark blue represent the read-out current responses after negative writing for 500 s, 50 s, 0, positive writing for 50 s, and 500 s, respectively. The corresponding currents of positive (c) and negative (d) readings for different t_w after 300 s. The detailed data (1, 5, 10, 50, 100, and 500 s of positive and negative writing time) for all positive (e) and negative (f) readings at 340 s as a function of the writing time are introduced. Red and blue symbols mark the reading current after negative and positive writings, respectively. The dashed line in black represents the current with 0 bias writing operations.

$$Z(t) = \left[1 - \frac{N(t)}{N_0}\right]\cdot\left[\left(\frac{1}{R_{2+}}\right)^2 + (\omega C_{2+})^2\right]^{-1/2} + \left[\frac{N(t)}{N_0}\right]\cdot\left[\left(\frac{1}{R_{3+}}\right)^2 + (\omega C_{3+})^2\right]^{-1/2} \quad (6)$$

where N_0 is the total number of Ni^{2+} and Ni^{3+} ions in the Ni-doped DNA device; $N(t)$ denotes the total number of Ni^{3+} ions; that is, $N(t)$ is a set of state variables (w) in eq 1 and 2, and R_{2+} (R_{3+}) is the equivalent resistance of the resistor network, where all Ni ions are in the Ni^{2+} (Ni^{3+}) state with all capacitances set to zero. C_{2+} (C_{3+}) is the equivalent capacitance of the capacitor network, where all Ni ions are in the Ni^{2+} (Ni^{3+}) state with all resistances set to zero (i.e., $r_{2+} = 0$ and $r_{3+} = 0$). In the absence of the capacitors, our model reduces to the memristor model,[15] where $Z(t)$ equals,

$$R(t) = [1 - N(t)/N_0]R_{2+} + [N(t)/N_0]R_{3+} \quad (7)$$

The diffusive current $\tilde{I}(t)$, which is proportional to the rate of change of Ni^{3+}, is expressed as:

$$\tilde{I}(t) = fe\frac{\partial}{\partial t}N(t) \quad (8)$$

where f is a parameter to be fitted by the experimental data. The value of f is typically large but can be justified by the equation of continuity shown in the Supporting Information. The rate of change in $N(t)$ is given by:

$$\frac{dN(t)}{dt} = k_{ox}(T, V(t))(N_0 - N(t)) - k_{red}(T, V)N(t) \quad (9)$$

where $k_{ox}(T,V(t))[k_{red}(T,V(t))]$ is the oxidation (reduction) rate constant. The rate constants are estimated using the modified Arrhenius rate equations:

$$k_{ox}(T, V(t)) = k_{ox}^0 \exp\left\{\frac{-\beta(E_{ox} - eV(t))}{\alpha T}\right\} \quad (10)$$

and

$$k_{red}(T, V(t)) = k_{red}^0 \exp\left\{\frac{(1-\beta)[(E_{red} - eV(t))]}{\alpha T}\right\} \quad (11)$$

respectively; k_{ox}^0(k_{red}^0) is the rate constant applicable when $E_{ox} = E_{red} = V(t) = 0$; E_{ox} (E_{red}) is the threshold energy required to trigger significant oxidation (reduction) reactions; β represents the symmetrization factor; α effectively describes the response of the rate constants to the external voltage due to multiple scatterings. When the Ni-doped DNA device is connected to a DC source at a voltage much larger than the activation energy, the oxidation (or reduction) reaction dominates. The steady DC current reduces the impedance Z to a resistance R_{3+} (R_{2+}) for positive (negative) voltages. The current can be used to estimate $R_{2+} = 4.5 \times 10^9\ \Omega$ and $R_{3+} = 2.25 \times 10^9\ \Omega$ for voltages fixed at ±6 V. The large resistances result in small drift currents of the order of ∼1 nA in the DC source.

The current in the cyclic $I-V$ characteristic is the sum of I_{drift} and $\tilde{I}$. The left panel of Figure 3a shows that $|I_{drift}(t)| \approx 100$ nA at around ±6 V. The drift current is enhanced by the capacitor effects due to the ω-dependent impedance in an AC source. The right panel of Figure 3a shows that $\tilde{I}(t) \approx 0$ for $|V(t)| \geq 6$ V due to the saturation of Ni^{3+} (or Ni^{2+}) ions. The left panel of Figure 3b compares the simulated cyclic $I-V$ curve with the experimental data at scan rate of 1 V/s, where the components of I_{drift} and $\tilde{I}$ are shown in the left and right panels of Figure 3b, respectively.

When the voltage is −9 V (or 9 V), the majority of Ni ions are in the Ni^{2+} (or Ni^{3+}) state. When the voltage is swept from −9 to 9 V (or 9 to −9 V), the dynamic process promotes an increase of the oxidation (or reduction) reaction rate. $\tilde{I}$ is positive (or negative) due to an increase (or decrease) in the number of Ni^{3+} ions due to oxidation (or reduction). In the voltage sweep range below $E_{ox}/e \approx 3.5$ V (or $E_{red}/e \approx -3.5$ V), the magnitude of $\tilde{I}$ increases gradually because the reaction still favors reduction (or oxidation). As the sweeping voltage exceeds the activation energy $E_{ox}/e \approx 3.5$ V (or $E_{red}/e \approx -3.5$ V), a drastic oxidation (or reduction) reaction of Ni ions is triggered with a rapid increase (or decrease) of $\tilde{I}$. $\tilde{I}$ is the dominant contributor to the cyclic $I-V$ characteristics and

reaches a maximum (or minimum) because $\partial N(t)/\partial t$ peaks at a voltage of $E_{p,a}/e \approx 5$ V (or $E_{p,b}/e \approx -5$ V). In the voltage range above $E_{p,a}/e$ (or $E_{p,c}/e$), the magnitude of $\tilde{I}$ decreases as the rate of change of ratio of Ni^{2+}/N^{3+} decreased. At voltages close to 9 V (or −9 V), we observe that $\tilde{I}(t) \approx 0$, given that $\partial N(t)/\partial t \approx 0$, where the majority of Ni ions are in the Ni^{3+} (or Ni^{2+}) state. Consequently, I_{drift} is dominant over $\tilde{I}$ in the cyclic $I-V$ curve at voltages around ±9 V. The simulated cyclic $I-V$ curves for various scanning rates are compared with the experimental data in the right panels of Figures 3b and 2a. The agreement between the simulated and the experimental data indicates the validity of this physical model. Therefore, the Ni-DNA system can be used as a memory device.

Interestingly, this Ni-DNA memory system can be set to operate in multiple states by using an operating voltage larger than the redox potential such as ±6 V, and controlling the writing time, t_w of applifying voltage. The set state of the Ni-DNA system can be read out at a reading voltage lower than the redox potential such as ±1 V. These reading voltages, ±1 V, are the optima condition for signal reading (Figure S5). Figure 4a shows the operation of writing voltage (blue and red lines for oxidized and reduced Ni ion states at ±6 V) and reading voltage (black lines with a ramp-up time t_r from 0 to ±1 V) supplied to the Ni-DNA memory with their corresponding current shown in Figure 4b. The current outputs of the Ni-DNA memory device present the black lines in Figure 4b without any writing operations. The read-out current reaches a stable current after 340 s. The positive (negative) reading of currents are represented by upward (downward) curves in red and in blue in Figure 4b after the negative writing of −6 V and the positive writing of +6 V, respectively. The writing times are 50 and 500 s. For the same positive reading, there is an apparent upward shift of the current after negative writing relative to that without writing operations, as indicated by black lines in Figure 4b. Figure 4c and d shows that the read-out currents reach stable gradually after 300−340 s. Namely, the I_{drift} is dominant at this reading period.

The number of writing states in the Ni-DNA memory system can be further increased. The multiple state behavior is attributed to a difference in the ratio of Ni^{3+} to Ni^{2+} ions in the Ni-DNA nanowires in response to different writing times. The operation of the Ni-DNA memory system in many states is prospectively achievable if the writing time and the writing process can be judiciously controlled. Figure 4e and f demonstrates the positive and negative reading of multiple states using different writing times, t_w. The dashed line indicates the current in the absence of a writing operation. Six writing operations were performed using various writing periods between 1 and 500 s, and the reading currents differed in the range from 47 (21) to 280 (213) pA between positive and negative writing states for the positive (negative) reading. The current difference beween the positive and negative writing states is larger for a longer period of writing time. The current difference could be differentiated even when more states of different writing time were incorporated. In fact, at least 10 different states could be individually identified from the positive and negative readings presented in Figures 4e and f. It is noted that the several points of deviation of the current readings from the expected result occur because the operation reset does not return precisely to the natural state of the Ni-DNA. These results demonstrate that Ni-DNA device can be operated as a multiple-state memory system. Different ratios of Ni^{3+} to Ni^{2+} ions in Ni-DNA can be generated under different writing conditions, leading to a multiple-state reading current due to a change in the Ni-DNA state resistance, $R(n(t_w,V),\ i)$. Accordingly, the Ni-DNA exhibits a great potential as a high-density memory device.

Figure 5 presents the erasing and reading current after the erasing. The erasing process is carried out after a positive/negative writing process. A sinusoidal driving voltage with an amplitude of 1.5 V is supplied to read the state. After a positive writing, the reading current shows a corresponding sinusoidal wave, while the current is shifted negatively with a central value at about −0.8 nA. The positive writing state can be totally erased by using the oscillating voltage, and after the erasing, the reading current shows a central value back to ∼0 nA. Alternatively, the erasing process is applied after a negative writing process. After the erasing, the reading current displays again a central value back to ∼0 nA. The results corroborate the erasing operation of multiple states in the Ni-DNA memory system.

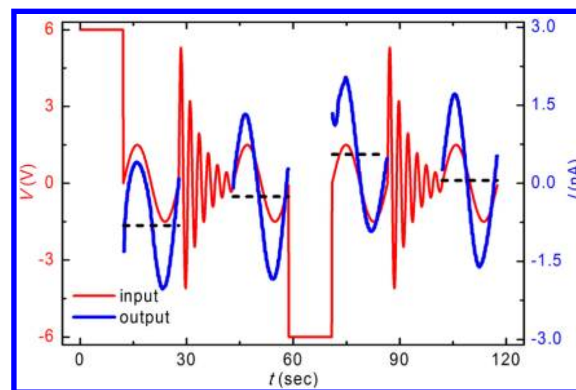

Figure 5. Operating voltage (red curves) and the corresponding current in the reading process (blue curves) as a function of time. For the first step, the positive writing of +6 V is carried out. It is then read by a sinusoidal wave to show current shifted to negative values. The following oscillating voltages erase the positive writing state, and the reading process displays a reading current back to a neutral state. The negative writing, reading process, and an erasing operation are demonstrated as well.

In conclusion, this study demonstrated that the conducting Ni ions chain can be formed in DNA and this two-terminal Ni-DNA device possesses a memristive effect that can be exploited in an organic multiple-state information storage device. The writing, reading, and erasing of information were demonstrated, which may be useful in several applications ranging from information storage to unconventional computing. Moreover, the similar self-assembled linear, two-dimensional, and three-dimensional lattices of DNA can be used as templates for future nanodevice fabrication.

Experimental Section. The chemicals, enzymes, BamHI and EcoRI DNA linkers, and the reagents in this study are described in the SI section. Rop-tat plasmid[18] was kindly provided by Dr. Ru-Chih C. Huang as a gift. The Rop DNA was digested with BamHI and EcoRI and metallized with Ni ions at pH 9.0 to form Ni-DNA as described in previous studies. The two terminal gold devices were fabricated with a standard lift-off procedure of semiconductors, and the gap width between each pair gold finger is 50−100 nm. The methods for SAMs of DNA linkers on the electrode surface can be obtained in our previous study[4,11] and the SI section. Ni-DNA from rop plasmids were connected with Ni-DNA linkers

on electrodes by overnight incubation at 4 °C and immersed in water with pH 9.0 five times. Once the Ni-DNA device was generated, the residue water on devices was removed by baking at 80 °C for 15 min. Electrical properties, including the current–voltage (I–V) behavior and memory effect, were characterized under ambient and water-free condition using a Keithley 6517b instrument with a two-probe configuration. For a detailed description, please see the SI section.

■ ASSOCIATED CONTENT

Supporting Information

Additional information on the Experimental Section with detailed procedures, patterned substrate of Ni-DNA device, Ni-DNA characterization, I–V characteristics of native DNA, justification of the form of the diffusive current, resistor–capacitor network model for the Ni-DNA nanowire system, and the optimal condition of reading bias voltages. This material is available free of charge via the Internet at http://pubs.acs.org.

■ AUTHOR INFORMATION

Corresponding Authors

*C.-C.C.: Tel.: +886-3-5731633. Fax: +886-3-5733259. E-mail: ccchang01@faculty.nctu.edu.tw.

*W.-B.J.: Tel.: +886-3-5712121-56159. Fax: +886-3-5725230. E-mail: wbjian@mail.nctu.edu.tw.

*Y.-C.C.: Tel.: +886-3-5131203. Fax: +886-3-5725230. E-mail: yuchangchen@mail.nctu.edu.tw.

Author Contributions

H.-L.C. and S.-C.C. contributed equally.

Notes

The authors declare no competing financial interest.

■ ACKNOWLEDGMENTS

This work was supported in part by the ATU-2 project of MOE, NSC project (NSC 100-2112-M-009-004-MY3), and AOARD-USAF award grant (FA2386-12-1-4042) for CCC. M.D. acknowledges partial support from the Center for Magnetic Recording Research at UCSD.

■ REFERENCES

(1) Aviram, A.; Ratner, M. A. *Chem. Phys. Lett.* **1974**, *29*, 277–283.

(2) Hwang, J. S.; Hwang, S. W.; Ahn, D. *Superlattices Microstruct.* **2003**, *34*, 433–438.

(3) Jangjian, P.-C.; Liu, T.-F.; Li, M.-Y.; Tsai, M.-S.; Chang, C.-C. *Appl. Phys. Lett.* **2009**, *94*, 043105–043103.

(4) Jian, P. C. J.; Liu, T. F.; Tsai, C. M.; Tsai, M. S.; Chang, C. C. *Nanotechnology* **2008**, *19*, 355703.

(5) Mirkin, C. A.; Letsinger, R. L.; Mucic, R. C.; Storhoff, J. J. *Nature* **1996**, *382*, 607–609.

(6) Porath, D.; Bezryadin, A.; de Vries, S.; Dekker, C. *Nature* **2000**, *403*, 635–638.

(7) de Pablo, P. J.; Moreno-Herrero, F.; Colchero, J.; Gómez, H. J.; Herrero, P.; Baró, A. M.; Ordejón, P.; Soler, J. M.; Artacho, E. *Phys. Rev. Lett.* **2000**, *85*, 4992–4995.

(8) Rakitin, A.; Aich, P.; Papadopoulos, C.; Kobzar, Y.; Vedeneev, A. S.; Lee, J. S.; Xu, J. M. *Phys. Rev. Lett.* **2001**, *86*, 3670–3673.

(9) Tseng, S. H.; JangJian, P. C.; Tsai, C. M.; Cheng, T. M.; Chu, H. L.; Chang, Y. C.; Chung, W. H.; Chang, C. C. *Biophys. J.* **2011**, *100*, 1042–1048.

(10) Dong, R.; Yan, X.; Li, K.; Ban, G.; Wang, M.; Cui, S.; Yang, B. *Nanoscale Res. Lett.* **2010**, *5*, 1431–1436.

(11) Jangjian, P.-C.; Liu, T.-F.; Tsai, C.-M.; Li, M.-Y.; Tsai, M.-S.; Tseng, S.-H.; Cheng, T.-M.; Chang, C.-C. *Chin. J. Phys.* **2009**, *47*, 740–747.

(12) Alexandre, S. S.; Soler, J.; Seijo, L.; Zamora, F. *Phys. Rev. B* **2006**, *73*, 205112.

(13) Periyasamy, G.; Collin, J. P.; Sauvage, J. P.; Levine, R. D.; Remacle, F. *Chem.—Eur. J.* **2009**, *15*, 1310–1313.

(14) Di Ventra, M.; Pershin, Y. V.; Chua, L. O. *Proc. IEEE* **2009**, *97*, 1717–1724.

(15) Strukov, D. B.; Snider, G. S.; Stewart, D. R.; Williams, R. S. *Nature* **2008**, *453*, 80–83.

(16) Xia, Q.; Robinett, W.; Cumbie, M. W.; Banerjee, N.; Cardinali, T. J.; Yang, J. J.; Wu, W.; Li, X.; Tong, W. M.; Strukov, D. B.; Snider, G. S.; Medeiros-Ribeiro, G.; Williams, R. S. *Nano Lett.* **2009**, *9*, 3640–3645.

(17) Pershin, Y. V.; Di Ventra, M. *Proc. IEEE* **2012**, *100*, 2071–2080.

(18) Giza, P. E.; Huang, R. C. C. *Gene* **1989**, *78*, 73–84.